

The Wind- and Wave-Driven Inner-Shelf Circulation

Steven J. Lentz¹ and Melanie R. Fewings²

¹Department of Physical Oceanography, Woods Hole Oceanographic Institution, Woods Hole, Massachusetts 02543; email: slentz@who.edu

²Marine Science Institute, University of California, Santa Barbara, California 93106; email: fewings@msi.ucsb.edu

Annu. Rev. Mar. Sci. 2012. 4:317–43

First published online as a Review in Advance on August 29, 2011

The *Annual Review of Marine Science* is online at marine.annualreviews.org

This article's doi:
10.1146/annurev-marine-120709-142745

Copyright © 2012 by Annual Reviews.
All rights reserved

1941-1405/12/0115-0317\$20.00

Keywords

coastal oceanography, cross-shelf exchange, upwelling, wave-current interaction, nearshore

Abstract

The inner continental shelf, which spans water depths of a few meters to tens of meters, is a dynamically defined region that lies between the surf zone (where waves break) and the middle continental shelf (where the along-shelf circulation is usually in geostrophic balance). Many types of forcing that are often neglected over the deeper shelf—such as tides, buoyant plumes, surface gravity waves, and cross-shelf wind stress—drive substantial circulations over the inner shelf. Cross-shelf circulation over the inner shelf has ecological and geophysical consequences: It connects the shore to the open ocean by transporting pollutants, larvae, phytoplankton, nutrients, and sediment. This review of circulation and momentum balances over the inner continental shelf contrasts prior studies, which focused mainly on the roles of along-shelf wind and pressure gradients, with recent understanding of the dominant roles of cross-shelf wind and surface gravity waves.

1. THE INNER CONTINENTAL SHELF

The inner shelf is the transition region between the surf zone and the middle of the shelf, typically spanning water depths from a few meters to a few tens of meters. Although there is general agreement that the inner shelf is bounded on the shoreward side by the outer edge of the surf zone, there have been numerous definitions for the offshore extent of the inner shelf that depend on the particular dynamics being considered (Garvine 2004). In this review, we use the term inner shelf to describe the region where the turbulent surface and bottom boundary layers together occupy the entire water column, similar to Lentz (1995). The width and location of the inner shelf vary in time, because the thicknesses of the surface and bottom boundary layers vary in time depending on the strengths of the wind and wave forcing and vertical density stratification.

A key feature of the inner shelf is the tendency for the cross-shelf circulation to decrease toward shore because of the presence of the coastal boundary and the substantial decrease in water depth: $\Delta b/b \approx 1$, where b is the water depth and Δb is the change in water depth across the inner shelf. The reduction in cross-shelf circulation toward the coast may limit the exchange of water across the inner shelf and the character of the exchange. The decrease in cross-shelf circulation and the substantial change in water depth can also result in vertical velocities that bring deeper water up toward the surface or carry surface water downward—coastal upwelling and downwelling. Exchange across the inner shelf and vertical transport are key elements in a wide range of interdisciplinary problems that motivate much of the research on inner-shelf circulation. The exchange of water masses across the inner shelf is important for transporting larvae, nutrients, low-oxygen water masses, sediment, and pollutants between the shore and the open ocean (Nittrouer & Wright 1994, Falkowski et al. 1998, Epifanio & Garvine 2001, Garland et al. 2002, Grantham et al. 2004, Dudas et al. 2009).

A wide variety of processes drive inner-shelf circulation, including winds, surface gravity waves, tides, and buoyant plumes. This review focuses on recent progress in understanding wind- and wave-driven flows over the inner shelf and particularly the circulations that result in vertical displacements and cross-shelf exchange. The focus is on subtidal frequencies: timescales of days to weeks, the timescales characteristic of weather systems that cause variations in wind and wave forcing.

2. DEPTH-AVERAGED FLOW

2.1. Continuity and Horizontal Velocities

Studies of inner-shelf circulation have to a large extent focused on depth-averaged flows and the associated dynamics. Subtidal, depth-averaged flows over the inner shelf tend to be strongly polarized in the along-shelf direction due to the constraint on cross-shelf flows imposed by the coastal boundary and the reduction in water depth. The polarization is evident in the relative sizes of the subtidal along-shelf (**Figure 1a**) and cross-shelf (**Figure 1b**) current variability over various continental shelves of the United States. Standard deviations of along-shelf subtidal currents range from 0.05 to 0.2 m s⁻¹ and do not exhibit any consistent dependence on water depth or offshore distance. Along-shelf flows over the inner shelf are not constrained by the coastal boundary and are as large over the inner shelf as over the middle and outer shelves (**Figure 1a**). In contrast, standard deviations of subtidal depth-averaged cross-shelf currents are much smaller (0.01–0.05 m s⁻¹) and increase with the distance offshore from near-zero values near the coast. The depth-averaged cross-shelf currents increase more rapidly with increasing water depth over the wider continental shelves of the east and south coasts of the United States (widths of approximately

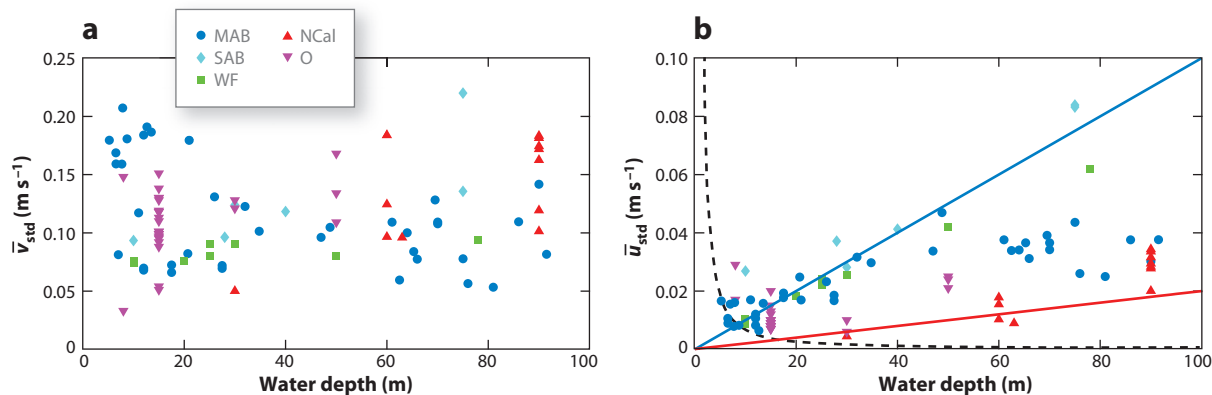


Figure 1

Standard deviations of the subtidal, depth-averaged (*a*) along-shelf currents v and (*b*) cross-shelf currents u as a function of water depth for five continental shelves: Middle Atlantic Bight (MAB; see figure 1 of Fewings et al. 2008 for data sets), South Atlantic Bight (SAB; Lee et al. 1984, 1989), West Florida (WF; Liu & Weisberg 2005), Northern California (NCal; Winant et al. 1987), and Oregon (O; Kirincich et al. 2009). The MAB, SAB, and WF shelves are relatively wide, whereas the NCal and O shelves are narrower with steeper bottom slopes. The solid blue and red lines in panel *b* are the predicted depth-averaged cross-shelf currents \bar{u}_{std} for the wide and narrow shelves, respectively, from Section 2.1. The black dashed line in panel *b* shows the predicted standard deviation of the depth-averaged Stokes drift \bar{u}_{st} (Equation 3) for wave forcing with a significant wave height of $H_s = 1$ m and a wave period of 8 s, typical of the east coast shelves. Note the different velocity scales in panels *a* and *b*. The along- and cross-shelf directions are defined by the major and minor principal axes of the subtidal depth-averaged flow, respectively.

100 km, bottom slopes of ~ 0.001) than over the narrower, steeper west coast shelf (widths of tens of kilometers, bottom slopes of ~ 0.01).

The magnitude of the fluctuations in the depth-averaged cross-shelf velocity, and their dependence on the water depth, can be explained by a simple scaling of the depth-averaged continuity equation

$$\frac{\partial(\bar{u}b)}{\partial x} + \frac{\partial(\bar{v}b)}{\partial y} = 0, \quad (1)$$

where x and y are the cross-shelf (positive onshore) and along-shelf coordinates, respectively, and \bar{u} and \bar{v} are the corresponding Eulerian depth-averaged velocities. To determine a scale for the cross-shelf flow based on the along-shelf flow, shelf slope, and water depth, we characterize the sizes of the variations in the cross- and along-shelf flows by \bar{u}_{std} and \bar{v}_{std} , respectively. We let L_y be a characteristic along-shelf scale for variations in \bar{v} and assume that L_y and \bar{v}_{std} are independent of x (as suggested by **Figure 1** for \bar{v}_{std}). Integrating Equation 1 from the coast to an offshore location x and using the coastal boundary condition $\bar{u}b = 0$ at $x = 0$ gives

$$\bar{u}_{\text{std}} \sim \frac{\bar{v}_{\text{std}} A}{L_y b} \sim \bar{v}_{\text{std}} \frac{b}{b_x L_y}, \quad (2)$$

where $A \sim xb \sim b^2/(b_x)$ is the cross-sectional area, and b_x is the bottom slope in the cross-shelf direction. Using $\bar{v}_{\text{std}} \approx 0.1 \text{ m s}^{-1}$ (**Figure 1a**) and $L_y \approx 100 \text{ km}$ (Kundu & Allen 1976, Dever 1997, Noble et al. 1983) and taking $b_x = 0.001$ for the wide shelves and $b_x = 0.005$ for the narrow shelves, we obtain reasonable estimates of both the magnitude and linear increase in \bar{u}_{std} (**Figure 1b**). This suggests that depth-averaged cross-shelf velocity fluctuations are associated with along-shelf variations in the along-shelf flow, presumably due to instabilities or along-shelf variations in the bathymetry or forcing. The depth-averaged cross-shelf flow increases with water depth or offshore distance and with decreasing bottom slope or L_y (Equation 2). The velocity

observations in **Figure 1** are from regions with relatively large L_y . In regions with bathymetric features such as capes, topographic bends such as Point Conception in California, or canyons, L_y will be much shorter, resulting in larger depth-averaged cross-shelf flows (e.g., Atkinson et al. 1986, Allen & Durrieu de Madron 2009).

2.2. Stokes Drift

There is a Stokes drift velocity associated with surface gravity waves that can be substantial over the inner shelf. The Stokes drift velocity arises because the wave orbital velocities vary in space as well as time (Stokes 1847). In a Lagrangian reference frame (following a water parcel), the wave orbital velocity is slightly larger at the top of the parcel's orbit than at the bottom; as a result, there is a net displacement of the water parcel—and associated volume transport—in the direction of wave propagation. In an Eulerian reference frame (fixed in space), the equivalent volume transport occurs above the wave troughs where there is alternately no water and water moving in the direction of wave propagation (Phillips 1980). The Stokes drift velocity can be estimated using linear wave theory as

$$\mathbf{u}_{\text{st}} = \frac{H_s^2 \omega k}{16} \frac{\cosh[2k(z+b)]}{\sinh^2(kb)} \hat{\mathbf{k}}, \quad (3)$$

where H_s is the significant wave height, ω is the angular wave frequency, $\mathbf{u}_{\text{st}} = (u_{\text{st}}, v_{\text{st}})$, k is the wave number, and $\hat{\mathbf{k}}$ is a unit wave vector (Stokes 1847, Mei 1983). The steady, depth-averaged continuity equation including the depth-averaged Stokes drift velocity is

$$\frac{\partial[(\bar{u} + \bar{u}_{\text{st}})b]}{\partial x} + \frac{\partial[(\bar{v} + \bar{v}_{\text{st}})b]}{\partial y} = 0. \quad (4)$$

The Stokes drift velocity must be explicitly included in the continuity equation because conventional current observations and models do not resolve surface gravity wave orbital velocities.

If we assume no along-shelf variations in the flow, then Equation 4 implies no cross-shelf variation in the cross-shelf transport. Because the net cross-shelf transport at the coast must be zero, the cross-shelf transport is zero everywhere and the vertically integrated continuity equation (Equation 4) reduces to

$$(\bar{u} + \bar{u}_{\text{st}})b = 0. \quad (5)$$

Therefore, for along-shelf uniform flow there should be an offshore depth-averaged flow that is equal in magnitude to the onshore depth-averaged Stokes drift velocity. Offshore transport driven by waves—referred to as undertow—is indeed observed in the surf zone, although the surf-zone relationship is complicated by additional onshore transport due to wave rollers associated with wave breaking (Haines & Sallenger 1994, Garcez Faria et al. 2000, Reniers et al. 2004). Two recent inner-shelf studies provided the first evidence for wave-driven cross-shelf flow over the inner shelf, showing close agreement between $-\bar{u}_{\text{st}}$ estimated from Equation 3 and observed \bar{u} in water depths of 15 m or less off Massachusetts, North Carolina (Lentz et al. 2008), and Oregon (Kirincich et al. 2009). At those shallow sites, depth-averaged cross-shelf flows \bar{u} are dominated by offshore flow events that are accurately predicted by $-\bar{u}_{\text{st}}$. The correlation between \bar{u} and $-\bar{u}_{\text{st}}$ decreases with increasing water depth, from 0.9 in 5–10-m water depth to near zero in approximately 20-m water depth. The decline in the correlation is consistent with the rapid decrease in \bar{u}_{st} as the water depth increases and with the increase in \bar{u}_{std} as the water depth increases (**Figure 1b**). For water depths greater than approximately 20 m and moderate wave heights, undertow accounts for a negligible fraction of depth-averaged cross-shelf current variability. Note that in the scaling analysis in Section 2.1, the depth-averaged Stokes drift should be added to the observed velocities \bar{u} to be

consistent with Equation 4. This was not done because the necessary wave measurements are not available for most of the observations. The missing depth-averaged Stokes drift may account for some of the larger cross-shelf velocity standard deviations in water depths of approximately 10 m in **Figure 1b**.

3. DEPTH-AVERAGED ALONG-SHELF MOMENTUM BALANCE

The depth-averaged along-shelf momentum balance provides insight into the dominant forces driving the along-shelf flow. A linearized form of the depth-averaged along-shelf momentum balance is

$$\frac{\partial \bar{v}}{\partial t} + f(\bar{u} + \bar{u}_{st}) = -\frac{1}{\rho_0 b} \int_{-b}^0 \frac{\partial P}{\partial y} dz + \frac{\tau^{sy} - \tau^{by}}{\rho_0 b} - \frac{1}{\rho_0 b} \left(\frac{\partial S^{xy}}{\partial x} + \frac{\partial S^{yy}}{\partial y} \right) - \frac{\tau^{bwy}}{\rho_0 b}, \quad (6)$$

where $f = 2\Omega \sin \theta_{lat}$ is the Coriolis frequency, Ω is the Earth's angular rotation rate, θ_{lat} is the latitude, ρ_0 is a reference seawater density, P is the pressure, z is the vertical coordinate, $z = 0$ is the mean water surface, τ^{sy} and τ^{by} are the along-shelf components of the surface and bottom stress, S^{xy} and S^{yy} are radiation stresses due to surface gravity waves (Longuet-Higgins & Stewart 1964), and τ^{bwy} is a bottom stress due to the waves (see Section 3.2) (Longuet-Higgins 1953). Both the nonlinear advection terms and terms involving interactions between the wave and mean flows (McWilliams et al. 2004, Smith 2006) may be substantial but are not included in Equation 6 for simplicity.

Recent awareness of the potential importance of surface gravity waves to shelf and open ocean dynamics has motivated a growing effort to include surface gravity wave forcing in numerical models (Mellor 2003, 2008; Ardhuin et al. 2004; McWilliams et al. 2004; Newberger & Allen 2006; Lane et al. 2007; Uchiyama et al. 2010). Surface gravity wave orbital velocities are typically not resolved either in numerical models of shelf circulation or by traditional observational techniques. Consequently, the effects of waves must be included as additional terms in the continuity (Equation 4) and momentum equations. The most notable change in recent studies of the inner-shelf momentum balance is the inclusion of the terms associated with surface gravity waves—the wave-radiation stresses, the Stokes-Coriolis term $f\bar{u}_{st}$, the wave-induced bottom stress, and corresponding terms in the cross-shelf momentum equation (see Section 4)—in both observational studies (Lentz et al. 1999, Fewings & Lentz 2010) and numerical models of shelf circulation (McWilliams et al. 2004, Newberger & Allen 2006, Smith 2006, Ardhuin et al. 2008, Mellor 2008, Uchiyama et al. 2010). However, because many studies of inner-shelf dynamics have not addressed the role of surface waves, we first discuss the along-shelf momentum balance in the absence of waves and then discuss the influence of waves.

3.1. Without Waves

In addition to neglecting the influence of waves, researchers often simplify the along-shelf momentum balance over the inner shelf by using a linear bottom drag law to represent the bottom stress and neglecting the Coriolis term $f\bar{u}$. Observational studies indicate that the Coriolis term $f\bar{u}$ is smaller than other terms over the inner shelf; on average, onshore of the 20-m isobath, the Coriolis term is less than half as large as the along-shelf wind stress term (**Figure 2b**). Even when $f\bar{u}$ is not negligible, studies in water depths of ~ 15 m or less indicate that $f\bar{u}$ can be balanced by the Stokes-Coriolis term ($f\bar{u}_{st}$; see Section 2.2) (Lentz et al. 2008, Kirincich et al. 2009, Fewings & Lentz 2010). Neglecting $f(\bar{u} + \bar{u}_{st})$ and the other wave-driven terms and representing the bottom stress using a linear drag law, $\tau^{by}/\rho_0 = r\bar{v}/b$, where r is the linear drag coefficient, one obtains

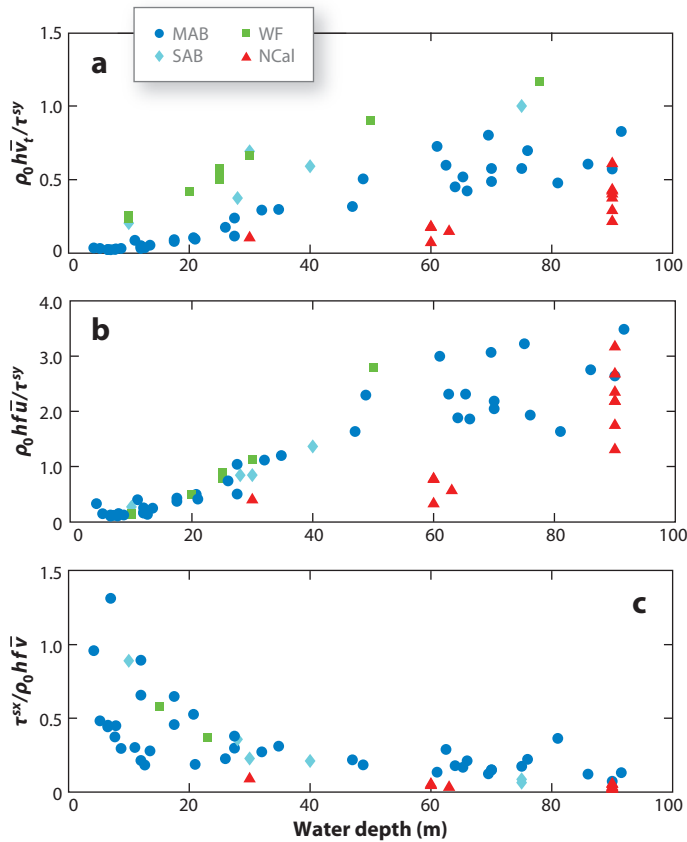


Figure 2

Ratios of the standard deviations of terms in the depth-averaged momentum balances (Equations 6 and 14) from four continental shelves. Along-shelf balance: (a) ratio of acceleration term to along-shelf wind stress term and (b) ratio of Coriolis term to along-shelf wind stress term. Cross-shelf balance: (c) ratio of cross-shelf wind stress term to Coriolis term. Data sets are the same as in **Figure 1**. Note the different vertical-axis scales. The cross-shelf wind stress is as large as the along-shelf wind stress on the Middle Atlantic Bight (MAB), South Atlantic Bight (SAB), and West Florida (WF) shelves. On the Northern California (NCal) shelf, cross-shelf winds are weak because the coastal mountain ranges force the near-surface winds to be oriented in the along-shelf direction. The depth-averaged along-shelf acceleration is \bar{v}_t , where subscript t indicates a time derivative. The seawater density is ρ_0 , the water depth is b , and the cross-shelf and along-shelf wind stresses are τ^{sx} and τ^{sy} , respectively. The depth-averaged cross-shelf velocity is \bar{u} , and f is the Coriolis parameter.

the along-shelf momentum balance

$$\frac{\partial \bar{v}}{\partial t} + \frac{r}{b} \bar{v} = -\frac{1}{\rho_0 b} \int_{-b}^0 \frac{\partial P}{\partial y} dz + \frac{\tau^{sy}}{\rho_0 b}, \quad (7)$$

which describes the development of the depth-averaged along-shelf flow in response to forcing by the along-shelf wind stress and pressure gradient. In this simple balance, the depth-averaged along-shelf flow accelerates until the bottom stress is large enough to balance the forcing.

The along-shelf momentum balance is further simplified over the inner shelf because the frictional timescale to reach steady state— $T_f = b/r$ for the linear drag law—decreases with

decreasing water depth. For a typical linear drag coefficient $r = 5 \times 10^{-4} \text{ m s}^{-1}$, T_f is approximately 1 day in 40 m of water. This suggests that for subtidal variability, the acceleration term $\partial \bar{v} / \partial t$ is small over the inner shelf. Indeed, in water shallower than 20 m, the acceleration term is typically observed to be less than half as large as the along-shelf wind stress (**Figure 2a**). Numerous observational studies indicate that the depth-averaged momentum balance is primarily among the three remaining terms: the wind stress, along-shelf pressure gradient, and bottom stress (Scott & Csanady 1976; Lee et al. 1984, 1989; Lentz & Winant 1986; Lentz 1994; Lentz et al. 1999; Liu & Weisberg 2005; Gutierrez et al. 2006; Fewings & Lentz 2010).

Although the along-shelf pressure gradient is treated as an independent forcing in Equation 7, it is part of the oceanic response to wind and other forcing. Inner-shelf studies suggest that along-shelf pressure gradients arise from a variety of processes. In some cases, along-shelf pressure gradients oppose the wind stress, consistent with a local response to spatial variations in the forcing and bathymetry (Lentz 1994, Yankovsky & Garvine 1998, Liu & Weisberg 2005, Kirincich & Barth 2009, Fewings & Lentz 2010). In other cases, the along-shelf pressure gradient is associated with remotely forced coastal-trapped waves that propagate along-shelf into the region (e.g., Lentz & Winant 1986, Hickey et al. 2003). Along-shelf pressure gradients may also be associated with buoyant plumes (Yankovsky & Garvine 1998, Lentz et al. 1999, Tilburg & Garvine 2003, Woodson et al. 2009).

As noted above, the bottom stress is a dominant term in the depth-averaged along-shelf momentum balance over the inner shelf and directly influences the magnitude of the along-shelf flow. Almost all studies cited above assume a linear or quadratic drag law with a constant drag coefficient. Commonly used models indicate, however, that the bottom shear stress and bottom drag over continental shelves depend on currents, waves, and sediment type and are affected by wave-current interactions in the centimeters-thick wave bottom boundary layer (Grant & Madsen 1979, 1986; Wiberg & Smith 1983; Styles & Glenn 2000), the development of bedforms (Grant & Madsen 1982, 1986; Wiberg & Harris 1994; Traykovski 2007), and stratification by suspended sediments (Glenn & Grant 1987). All these processes are likely important over the shallow inner shelf, where near-bottom wave orbital velocities are often large and vary rapidly in the cross-shelf direction because surface waves are propagating into shallower water (shoaling). For example, a wave-current interaction model (Grant & Madsen 1986) in 10-m water depth with moderate wind forcing ($\tau^{xy} = 0.1 \text{ N m}^{-2}$) predicts that strong wave forcing typical of U.S. east coast storms ($H_s = 3 \text{ m}$, wave period of 6 s) produces a fourfold increase in the quadratic drag coefficient and a factor-of-two reduction in the along-shelf flow. Despite the substantial impact of surface waves on the bottom stress suggested by models, only a few inner-shelf observational or modeling studies have considered the influence of wave-current interactions on bottom stress (Keen & Glenn 1994, Gutierrez et al. 2006, Fewings & Lentz 2010).

3.2. With Waves

The terms in the along-shelf momentum balance (Equation 6) due to surface gravity waves are roughly analogous to turbulent Reynolds stresses and represent mean (over periods long compared with the wave period) momentum fluxes due to the waves. The wave forcing can be expressed using a vortex-force representation (McWilliams et al. 2004, Lane et al. 2007, Ardhuin et al. 2008); in Equation 6, we represent it more traditionally as divergences in the wave-radiation stresses S^{xy} and S^{yy} (Longuet-Higgins & Stewart 1964), the Stokes-Coriolis acceleration $f \bar{u}_{st}$ (Hasselmann 1970, Xu & Bowen 1994), and a near-bottom stress due to the waves τ^{bwy} (Longuet-Higgins 1953). There may also be surface stresses associated with waves and whitecapping that are often assumed to be part of the wind stress (Uchiyama et al. 2010).

The radiation stresses include momentum fluxes due to both the wave velocities (such as a term proportional to $\langle u_w u_w \rangle$, where u_w is the wave orbital velocity and $\langle \rangle$ indicates a time average over many wave periods) and the wave pressure fluctuations (Longuet-Higgins & Stewart 1964). The radiation stress terms in Equation 6, estimated using linear wave theory, may be written as

$$\begin{aligned} S^{xy} &= E \frac{c_g}{c} \cos \theta_w \sin \theta_w, \\ S^{yy} &= E \left[\frac{c_g}{c} (\sin^2 \theta_w + 1) - \frac{1}{2} \right], \end{aligned} \quad (8)$$

where $E = \rho_0 g H_s^2 / 16$ is the wave energy; g is the acceleration due to gravity; c_g and c are the group velocity and phase speed of the waves; and θ_w is the direction the waves are propagating, measured counterclockwise from the $+x$ direction, so $\theta_w = 0$ for waves propagating onshore (Longuet-Higgins & Stewart 1964, Mei 1983).

The bottom wave stress τ^{bwy} results from bottom friction causing v_w and w_w to be slightly in phase in the wave bottom boundary layer. The result is a wave stress $\rho_0 \langle v_w w_w \rangle$ that causes near-bottom wave streaming or flow in the direction of wave propagation (Longuet-Higgins 1953, Xu & Bowen 1994, Zou et al. 2006).

The other wave forcing term in Equation 6 is the Stokes-Coriolis acceleration $f \bar{u}_{st}$. The Stokes-Coriolis acceleration is a consequence of the influence of the Earth's rotation on surface gravity waves (Ursell 1950, Hasselmann 1970, Xu & Bowen 1994). The Coriolis force causes a slight deflection of the wave orbital velocity (to the right in the Northern Hemisphere). The resulting along-crest velocity is small ($v_w = f u_w / \omega \approx 10^{-4} u_w$ for waves propagating in the x direction), but because it is 90° out of phase with the horizontal velocity u_w , it is in phase with the vertical velocity w_w . Consequently, there is a nonzero vertical momentum flux divergence:

$$\rho_0 \frac{\partial \langle v_w w_w \rangle}{\partial z} = \rho_0 f u_{st}.$$

This Stokes-Coriolis term can be similar in magnitude to the wind stress term (McWilliams & Restrepo 1999). The turbulent stress (per unit density) associated with winds $\langle v' w' \rangle$ is approximately 10^{-4} m s^{-2} because the turbulent velocity fluctuations are $v' \approx w' \approx 10^{-2} \text{ m s}^{-1}$. The Stokes-Coriolis stress (per unit density) $\langle v_w w_w \rangle$ is also approximately 10^{-4} m s^{-2} because $v_w \approx 10^{-4} \text{ m s}^{-1}$ and $w_w \approx 1 \text{ m s}^{-1}$.

To focus on wave-forced flows over the inner shelf, we assume no along-shelf variations and no wind stress and neglect acceleration (as discussed in Section 3.1). Then $\bar{u} = -\bar{u}_{st}$ from the continuity equation (Equation 5), and the along-shelf momentum balance (Equation 6) reduces to

$$0 = -\frac{\tau^{by}}{\rho_0 b} - \frac{1}{\rho_0 b} \left(\frac{\partial S^{xy}}{\partial x} \right) - \frac{\tau^{bwy}}{\rho_0 b}. \quad (9)$$

If the waves propagate directly onshore, so $\theta_w = 0$, then S^{xy} (Equation 8) and τ^{bwy} are zero and therefore $\tau^{by} = 0$, implying that there is no along-shelf flow. If waves approach the coast at an angle, the wave-radiation stress and wave bottom stress are nonzero. In the surf zone, waves approaching the coast at an angle result in a large cross-shelf gradient in S^{xy} that accelerates an along-shelf flow until the bottom stress τ^{by} balances the radiation stress gradient in Equation 9 (Thornton & Guza 1986). In the few studies that consider wave forcing over the inner shelf, cross-shelf gradients in S^{xy} are assumed to be zero outside the surf zone (Lentz et al. 1999, Fewings & Lentz 2010). This results from the assumption that wave dissipation is negligible where

waves are not breaking. Let us assume that surface gravity waves obey Snell's law,

$$\frac{\partial}{\partial x} \left(\frac{\sin \theta_w}{c} \right) = 0, \quad (10)$$

as they propagate across isobaths and assume that cross-isobath changes in wave-energy flux result only from dissipation ϵ :

$$\frac{\partial}{\partial x} (c_g E \cos \theta_w) = -\epsilon. \quad (11)$$

Using Equations 10 and 11 in Equation 8, we obtain

$$\frac{\partial S^{xy}}{\partial x} = \frac{\partial (E c_g \cos \theta_w)}{\partial x} \frac{\sin \theta_w}{c} + E c_g \cos \theta_w \frac{\partial}{\partial x} \left(\frac{\sin \theta_w}{c} \right) = -\frac{\epsilon \sin \theta_w}{c}. \quad (12)$$

This implies that there is a cross-shelf gradient in S^{xy} if there is wave dissipation and waves approach the coast at a nonzero angle.

Although wave dissipation has been neglected in inner-shelf studies, there can be substantial dissipation of wave energy by whitecapping or bottom stress. Recent studies suggest that even in low-wind conditions (no whitecapping) there can be substantial dissipation across broad shallow shelves due to bottom drag associated with sand ripples (Herbers et al. 2000, Ardhuin et al. 2001). If the wave dissipation over the inner shelf results from bottom drag such that $\epsilon = c |\boldsymbol{\tau}^{bw}|$ (Longuet-Higgins 2005), it follows from Equation 12 that

$$\frac{\partial S^{xy}}{\partial x} = |\boldsymbol{\tau}^{bw}| \sin \theta_w = -\tau^{bwy}.$$

Then Equation 9 again yields $\tau^{by} = 0$, implying that the only wave-driven along-shelf velocity is the along-shelf component of the bottom streaming velocity, which for a constant viscosity laminar flow is (Longuet-Higgins 1953)

$$\mathbf{u}_{bs} = \frac{5}{32} \frac{H_s^2 \omega^2}{c \sinh^2(kb)} \hat{\mathbf{k}}. \quad (13)$$

The along-shelf component $|\mathbf{u}_{bs}| \sin \theta_w$ is typically small compared with along-shelf flows driven by winds and pressure gradients. Bottom streaming in a turbulent wave boundary layer is reduced and may even reverse direction compared with Equation 13 (Davies & Villaret 1999).

4. DEPTH-AVERAGED CROSS-SHELF MOMENTUM BALANCE: COASTAL SETUP AND SETDOWN

The depth-averaged cross-shelf momentum balance provides insight into the causes of cross-shelf pressure gradients and the associated setup or setdown of the sea level near the coast. Assuming that depth-averaged along-shelf flows are large compared with depth-averaged cross-shelf flows (consistent with **Figure 1**), focusing on subinertial frequencies (timescales longer than f^{-1}), and neglecting the nonlinear inertial terms, we find that the depth-averaged cross-shelf momentum balance is

$$\frac{1}{\rho_0 b} \int_{-b}^0 \frac{\partial P}{\partial x} dz = f(\bar{v} + \bar{v}_{st}) + \frac{\tau^{sx} - \tau^{bx}}{\rho_0 b} - \frac{1}{\rho_0 b} \left(\frac{\partial S^{xx}}{\partial x} + \frac{\partial S^{yx}}{\partial y} \right) - \frac{\tau^{bwx}}{\rho_0 b}. \quad (14)$$

If we assume that the contribution of cross-shelf density gradients to the pressure gradient is small in shallow water (for example, neglecting the influence of buoyant plumes), then $\partial P / \partial x \approx g \partial \eta / \partial x$, where η is the sea level. Then over the shelf, Equation 14 is an expression for the cross-shelf gradient in the sea level and hence the coastal setup or setdown due to winds,

waves, and the geostrophic along-shelf flow (Tilburg & Garvine 2004, Liu & Weisberg 2007, Fewings & Lentz 2010). Although cross-shelf wind stress and wave-radiation stresses due to unbroken, shoaling surface waves are typically negligible over the middle and outer shelves, those terms can be important over the inner shelf because in Equation 14 they increase relative to the Coriolis term as the water depth b decreases.

4.1. Geostrophy

Over the middle and outer shelves, the cross-shelf momentum balance tends to be dominated by the geostrophic terms—a balance between the Coriolis acceleration associated with the along-shelf flow ($-f\bar{v}$) and the cross-shelf pressure gradient term (Brown et al. 1985, 1987; Lee et al. 1989; Shearman & Lentz 2003; Liu & Weisberg 2005). For depth-averaged along-shelf current variations $O(0.1 \text{ m s}^{-1})$ on a mid-latitude shelf ($f = 10^{-4} \text{ s}^{-1}$) of width $O(100 \text{ km})$, the hydrostatic relation and geostrophy suggest that the sea-level difference between the shelf edge and the coast due to geostrophic balance is $O(10 \text{ cm})$. The associated sea-surface slope over the inner shelf will generally be similar to the middle and outer shelves because the depth-averaged along-shelf current fluctuations are similar (Figure 1a).

4.2. Cross-Shelf Wind

The cross-shelf wind stress term in Equation 14 is a substantial fraction of the Coriolis term in water depths less than approximately 30 m on continental shelves where cross-shelf and along-shelf wind stresses have similar magnitudes (Figure 2c). The cross-shelf wind term is rarely larger than the Coriolis term, however.

The cross-shelf pressure gradient or sea-level slope due to cross-shelf winds should be confined to the region onshore of where the surface boundary layer extends to the bottom. In deeper water, one expects an Ekman (1905) balance between the cross-shelf wind stress and the Coriolis term associated with the wind-driven along-shelf transport in the surface boundary layer V^E so that $-fV^E = \tau^{sx}/\rho_0$, and there is no cross-shelf pressure gradient. In shallower water, where fV^E is small, the sea-surface slope due to the cross-shelf wind stress is (Nof & Paldor 1992)

$$\partial\eta/\partial x \approx \frac{\tau^{sx}}{\rho_0 g b}.$$

Integrating from the water depth $b = \delta_s$ where the surface boundary layer intersects the bottom to the offshore edge of the surf zone where $b = b_{sz}$ yields

$$\Delta\eta \approx \frac{\tau^{sx}}{\rho_0 g b_x} \ln\left(\frac{b_{sz}}{\delta_s}\right).$$

The singularity at $b_{sz} = 0$ can be removed by not assuming $\eta \ll b$ and instead replacing b by $\eta + b$ (Nof & Paldor 1992). This wind-driven setup does have a weak dependence on stratification because stratification reduces the surface boundary-layer thickness δ_s . For a moderate wind stress $\tau^{sx} = 0.1 \text{ N m}^{-2}$ on a gently sloping shelf ($b_x = 0.001$), the setup or setdown is a few centimeters, whereas for a hurricane-force wind stress ($\tau^{sx} = 1 \text{ N m}^{-2}$), the setup can be 0.5 m or more (Drinkwater 1989).

4.3. Waves

Within the surf zone, owing to waves propagating onshore and breaking, there is a large cross-shelf gradient in the onshore momentum flux that may be estimated using linear wave theory to

calculate the wave-radiation stress (Longuet-Higgins & Stewart 1964):

$$S^{xx} = E \left[\frac{c_g}{c} (\cos^2 \theta_w + 1) - \frac{1}{2} \right]. \quad (15)$$

The cross-shelf gradient of the wave-radiation stress is primarily balanced by a cross-shore pressure gradient, so that $\partial S^{xx}/\partial x \approx -b \partial P/\partial x$ in Equation 14 (Bowen et al. 1968, Raubenheimer et al. 2001). The associated wave-driven setup of the coastal sea level from the outer edge of the surf zone to the coast is typically tens of centimeters (Bowen et al. 1968, Raubenheimer et al. 2001).

Over the inner shelf, where waves are not breaking, radiation stress gradients can be caused by wave shoaling. The resulting wave-radiation stress gradients are typically an order of magnitude smaller than those in the surf zone but can still be substantial relative to the Coriolis term and the cross-shelf wind stress over the inner shelf (Lentz et al. 1999). Theoretical and laboratory studies indicate that if there is no dissipation of wave energy, then shoaling waves drive a setdown of the sea level toward the coast (Bowen et al. 1968). This follows again from the assumption that the cross-isobath changes in wave-energy flux result only from dissipation. If there is no wave dissipation, the wave-energy flux is conserved ($\epsilon = 0$ in Equation 11). Because c_g decreases as the water depth decreases for $kb < 1$, the wave energy E —and the wave height, because $E \propto H_s^2$ —must increase. Consequently, the wave-radiation stress S^{xx} (Equation 15) increases as the water becomes shallower. The resulting wave-radiation stress gradient is balanced by a cross-shelf pressure gradient

$$gb \frac{\partial \eta}{\partial x} = -\frac{\partial S^{xx}}{\partial x},$$

corresponding to a setdown of the sea level toward the coast.

There can be substantial dissipation across broad shallow shelves due to the bottom drag (see Section 3.2) (Herbers et al. 2000). Longuet-Higgins (2005) showed that for a cross-shelf momentum balance given by

$$g \frac{\partial \eta}{\partial x} = -\frac{1}{\rho_0 b} \left(\frac{\partial S^{xx}}{\partial x} \right) - \frac{\tau^{bwx}}{\rho_0 b}, \quad (16)$$

there is a local wave-driven setdown—relative to the sea level in the absence of wave forcing—given by

$$\eta = -\frac{1}{16} \frac{H_s^2 k}{\sinh(2kb)}. \quad (17)$$

This is a local balance representing the tendency for the sea level to be depressed under waves (Longuet-Higgins & Stewart 1962) and is also referred to as the quasi-static component of the sea-level response to the waves (McWilliams et al. 2004). Although dissipation does not appear explicitly in Equation 17, it does influence H_s and can have a substantial impact on the wave-driven setdown. With no dissipation, the predicted setdown is 1–3 cm in water depths of 5–10 m for $H_s = 2$ m. For a dissipation that reduces the significant wave height by a factor of two across the shelf [as observed for the Middle Atlantic Bight (Herbers et al. 2000)], the setdown is less than 1 cm. Only a few observational studies have considered wave-radiation stresses in inner-shelf momentum balances. Just outside the surf zone, the observed and predicted sea-level setdown due to $\partial S^{xx}/\partial x$ are in close agreement (Raubenheimer et al. 2001). In 12–13-m water depth, the estimated cross-shelf gradient in radiation stress is as large as the Coriolis and cross-shelf wind stress terms (Lentz et al. 1999, Fewings & Lentz 2010), although in the latter study $\partial S^{xx}/\partial x$ was uncorrelated with the observed cross-shelf pressure gradient.

There are three other wave-driven terms in the cross-shelf momentum balance (Equation 14). The first term—an along-shelf gradient in the wave-radiation stress $S^{yx} = S^{xy}$ (Equation 8)—depends on along-shelf variations in the wave field, which are not well studied. The second is the Stokes-Coriolis term. When waves propagate onshore at a nonzero angle, the component of the Stokes-Coriolis term that appears in the cross-shelf balance ($f\bar{v}_{st}$) is not zero, but it was small compared with the Coriolis and cross-shelf wind stress terms in the one study that considered it (Fewings & Lentz 2010). The third term, involving the wave-induced bottom stress τ^{bwx} , drives the cross-shelf component of the bottom streaming velocity $|\mathbf{u}_{bs}| \cos \theta_w$ (Equation 13). A recent modeling study suggests that bottom streaming can have a substantial impact on the cross-shelf velocity profile over the inner shelf (Uchiyama et al. 2010).

5. VERTICAL STRUCTURE OF THE CROSS-SHELF CIRCULATION

5.1. Wind-Driven Circulation

Vertical structure in the cross-shelf circulation can result in substantial cross-shelf exchange and is not represented by the depth-averaged flows and associated momentum balances discussed above. In this section we focus on simple along-shelf uniform wind-driven circulation so that there is onshore or offshore flow in the upper water column and a compensating return flow in the lower water column.

Ekman (1905) developed the first model of wind-driven circulation over a sloping continental shelf that included the influence of the Earth's rotation. In deep water, the steady, wind-driven (Ekman) volume transport in the surface boundary layer is $|\boldsymbol{\tau}^s|/(\rho_0 f)$ and in the Northern Hemisphere is 90° to the right of the wind stress $\boldsymbol{\tau}^s$. The transport is confined to a surface boundary layer with a thickness characterized by the Ekman scale $\delta_E = \sqrt{2A/f}$ (for a constant eddy viscosity A). Where the water depth is less than δ_E , as the water depth decreases, the transport perpendicular to the wind stress decreases. In the region where $b \ll \delta_E$, the transport is entirely in the direction of the wind stress, as expected for a nonrotating fluid. Ekman assumed a steady, linear, along-shelf uniform wind-driven circulation. The cross-shelf and along-shelf momentum equations in that case are

$$-\rho_0 f v = -\frac{\partial P}{\partial x} + \frac{\partial \tau^x}{\partial z} \quad (18)$$

and

$$\rho_0 f u = \frac{\partial \tau^y}{\partial z}. \quad (19)$$

Ekman solved for the circulation by linearly superimposing the solutions for a wind stress and a cross-shelf pressure gradient and then requiring the net cross-shelf transport to be zero everywhere to satisfy volume conservation ($\bar{u}b = 0$ from Equation 5 with $\bar{u}_{st} = 0$). Estrade et al. (2008) provided a nice modern derivation of Ekman's solution for a continental shelf. A key feature of the solutions is that the circulation depends only on U^E , δ_E , b , and z . Ekman assumed a constant eddy viscosity A to relate the stress to the vertical shear ($\boldsymbol{\tau}^s = A\partial\mathbf{u}/\partial z$), allowing a relatively simple analytic solution. A more realistic approach is to assume a turbulent eddy viscosity that depends on the applied surface and bottom stresses and distance from the surface and bottom boundaries (Thomas 1975, Poon & Madsen 1991, Lentz 1995). In that case, the Ekman layer scale is $\delta_{Et} \sim \kappa u_* / f$, where $\kappa \approx 0.4$ is von Kármán's constant and $u_* = \sqrt{|\boldsymbol{\tau}|/\rho_0}$ is the shear velocity (Madsen 1977). As in the constant eddy-viscosity case, the turbulent eddy-viscosity solutions depend only on U^E , δ_{Et} , b , and z . Below we discuss the responses to along-shelf and cross-shelf wind stresses in the context of turbulent eddy viscosities because the scalings are slightly different from the constant

eddy-viscosity solutions. Nevertheless, Ekman's original solutions capture the key features of the inner-shelf response to both along-shelf and cross-shelf wind forcing for unstratified flow.

5.2. Along-Shelf Wind Forcing

For the case of an unstratified continental shelf exposed to along-shelf wind forcing, analytical solutions exist for the cross- and along-shelf circulation responses if a simple eddy-viscosity profile is assumed. A downwelling-favorable along-shelf wind stress over an along-shelf uniform unstratified water column forces a steady cross-shelf circulation pattern with onshore flow near the surface and an offshore return flow near the bottom (**Figure 3**) (Ekman 1905). The linear, unstratified, along-shelf uniform response is symmetric with respect to wind stress direction, so reversing the wind stress to upwelling-favorable just reverses the circulation pattern. There is a convergence in the onshore transport in the surface boundary layer as the water depth decreases ($b < 2\delta_s$, where $\delta_s \propto \delta_{Et}$ is the boundary-layer thickness) that initially causes sea level to rise toward the coast (and leads to the geostrophic setup discussed in Section 4). In deep water, where the surface and bottom boundary layers do not overlap so there is an interior region without turbulent stresses, the resulting cross-shelf pressure gradient balances a geostrophic along-shelf flow (Equation 18 neglecting the stress term). The bottom stress due to the geostrophic along-shelf flow drives the offshore flow (Ekman transport) in the bottom boundary layer that compensates for the onshore surface flow. In shallow water where the surface and bottom boundary layers do overlap, the surface stress is transmitted directly to the bottom by turbulent momentum fluxes.

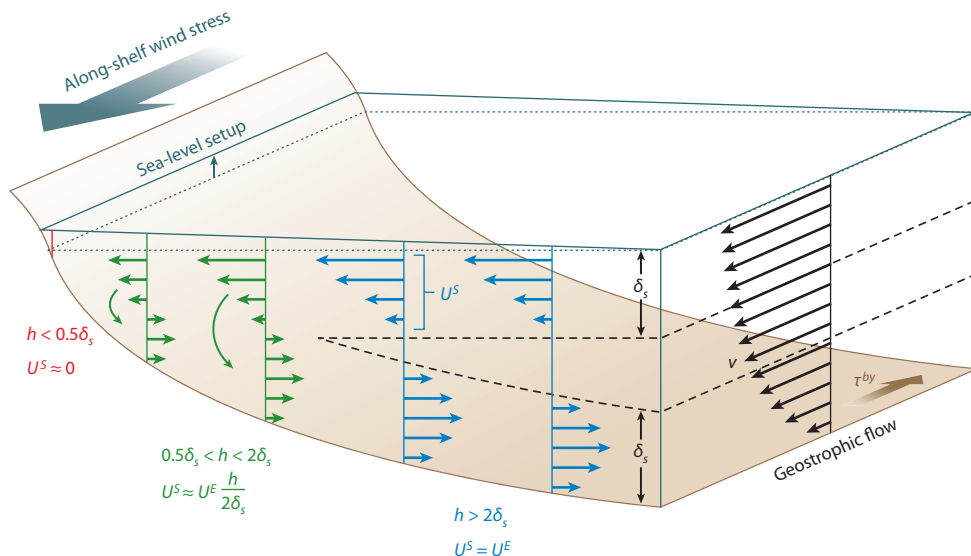


Figure 3

Schematic of the unstratified inner- and middle-shelf responses to an along-shelf wind stress, highlighting dynamical regions onshore and offshore of the locations where the surface and bottom boundary layers interact: very shallow water (*red*), intermediate region (*green*), and middle shelf (*blue*). The geostrophic setup of the sea level extends across the shelf. The water depth is b , the surface and bottom boundary-layer thicknesses are δ_s , the along-shelf velocity is v , the along-shelf component of the bottom stress is τ^{by} , the cross-shelf volume transport in the surface boundary layer is U^S , and the Ekman transport driven by the along-shelf wind in deep water is $U^E = \tau^{sy} / \rho_0 f$, where ρ_0 is the seawater density and f is the Coriolis parameter.

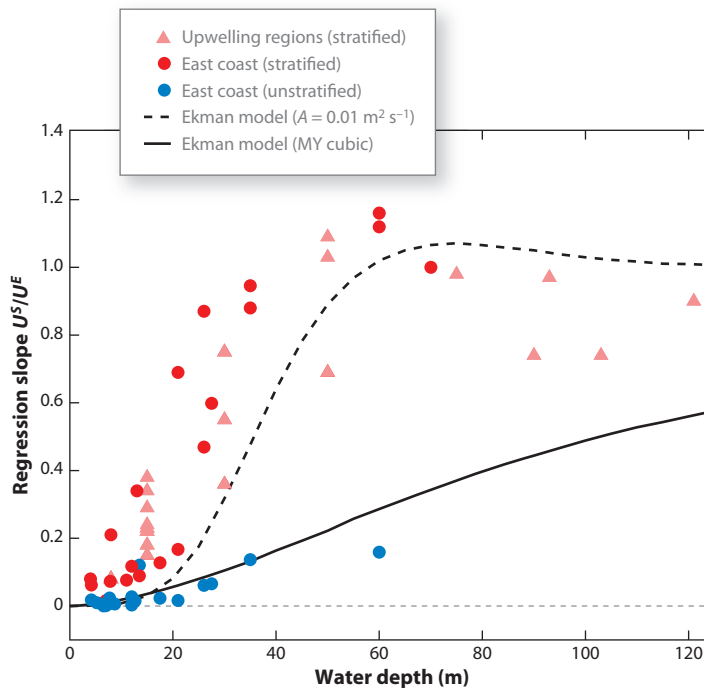


Figure 4

Linear regression slope between observed cross-shelf transport in the surface boundary layer (U^S) and the Ekman transport estimated from the along-shelf wind stress (U^E) as a function of water depth for locations on the east coast of the United States and from coastal upwelling regions (Lentz 1992, Lentz 2001, Shearman & Lentz 2003, Kirincich et al. 2005, Lentz et al. 2008). Estimates are also shown from an along-shelf uniform, unstratified model (Lentz 1995) for a constant eddy viscosity (A) and a cubic eddy viscosity (MY cubic) that resembles a Mellor-Yamada (Mellor & Yamada 1982) parameterization for unstratified flow (see Fewings et al. 2008).

The resulting steady circulation consists of three regions (**Figures 3 and 4**). Over the middle shelf, where the surface and bottom boundary layers are separated—roughly $h > 2\delta_s$ —there is a constant onshore transport in the surface boundary layer $U^S = U^E$ and an equal offshore transport in the bottom boundary layer (Lentz 2001), separated by a geostrophic interior. In very shallow water (roughly $h < 0.5\delta_s$), the stress is approximately constant throughout the water column ($\partial\tau^y/\partial z \approx 0$ in Equation 19), so there is essentially no cross-shelf circulation ($U^S \approx 0$) and the flow is downwind, consistent with a nonrotating fluid. In the intermediate region, where δ_s is similar to the water depth ($0.5\delta_s > h > 2\delta_s$), the cross-shelf transport increases approximately linearly with increasing water depth. In this region, the convergence in the onshore transport implies that there must be a vertical velocity—downwelling or upwelling—to conserve mass (Lentz 1995, Estrade et al. 2008). The inclusion of an along-shelf pressure gradient results in a similar response with the addition of a geostrophic cross-shelf flow in the interior (Ekman 1905, Lentz 1995).

Stratification profoundly affects the inner-shelf response to along-shelf wind forcing. The most obvious impact is that the region where the surface and bottom boundary layers interact—resulting in a reduction of the cross-shelf circulation—occurs in shallower water because stratification inhibits vertical mixing (e.g., see Lentz 2001, figure 3). However, because of the dynamical relationships among stratification, vertical mixing, and cross-shelf circulation, the effect of stratification

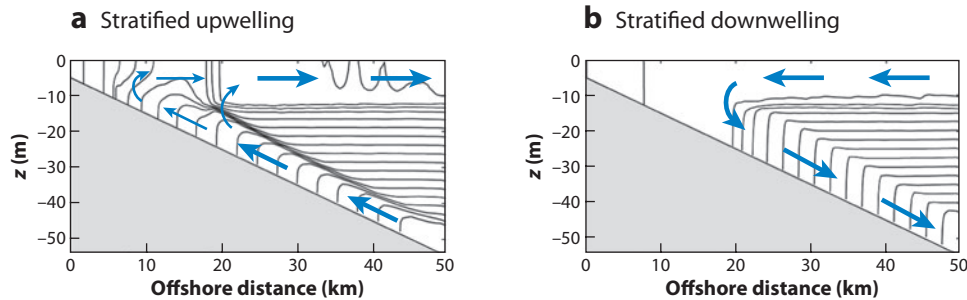


Figure 5

Schematics of the stratified inner- and middle-shelf responses to an along-shelf wind stress, highlighting the difference between (a) upwelling and (b) downwelling. The gray contours are lines of constant density. Blue arrows indicate cross-shelf circulation. Figure modified with permission from Austin & Lentz (2002).

on the inner-shelf response to along-shelf wind forcing is more complicated than a reduction in boundary-layer thicknesses (Keen & Glenn 1994, Allen et al. 1995, Allen & Newberger 1996, Austin & Lentz 2002, Tilburg 2003). For the case of a stratified continental shelf exposed to along-shelf wind forcing, the cross-shelf circulation response has not been found analytically, except in idealized models that do not include an inner shelf (Pedlosky 1978; Choboter et al. 2005, 2011). Numerical modeling studies of the response of a stratified shelf to along-shelf wind stress suggest the formation of two regions with very different responses. The two regions, which are separated by an enhanced horizontal density gradient—an upwelling or downwelling front—are a stratified middle to outer shelf and an inner shelf that is unstratified or weakly stratified (Figure 5). In contrast to the unstratified response, stratification results in an asymmetry in the response to upwelling-favorable and downwelling-favorable wind stresses.

For downwelling-favorable winds blowing over a stratified shelf, models suggest that the onshore flow in the surface boundary layer combines with vertical mixing to form an unstratified inner-shelf region where the cross-shelf circulation is very weak (Figure 5b) (Allen & Newberger 1996, Austin & Lentz 2002). The inner-shelf region remains unstratified because it is fed with homogeneous water from the surface mixed layer, and the very weak cross-shelf circulation continually forces the density field toward convective instability (denser water above less dense water). In the stratified region on the middle and outer shelves, there is a robust cross-shelf circulation with offshore flow in the bottom boundary layer. The divergence in the cross-shelf circulation and the resulting downwelling are concentrated at the downwelling front between the stratified shelf water and the unstratified inner shelf where the cross-shelf circulation is shut down. The downwelling front moves offshore at a rate consistent with the onshore transport of mixed surface boundary-layer water (Austin & Lentz 2002). The shutdown of the cross-shelf circulation means that during downwelling on a stratified shelf, the inner shelf and surf zone are isolated from exchange with the stratified middle-shelf water. Drifters on the Oregon shelf during downwelling-favorable winds were observed to stop moving onshore well away from the coast and instead moved in the along-shelf direction, consistent with these model predictions (Austin & Barth 2002).

For upwelling-favorable winds blowing over a stratified shelf, models again indicate that the middle shelf is separated by a front from an inner-shelf region with weaker stratification. In contrast to the downwelling case, the cross-shelf circulation onshore of the upwelling front is not completely shut down. Offshore of the front, there is offshore flow in the surface boundary layer and onshore flow in the bottom boundary layer (Figure 5a) (Allen et al. 1995, Austin & Lentz 2002). As in the downwelling case, the upwelling front moves offshore at a rate consistent with

the offshore transport in the surface boundary layer. In the upwelling case, however, stratification is maintained onshore of the front because the density of the water transported onshore in the bottom boundary layer increases as it is drawn from deeper depths along the sloping bottom. The resulting stratification over the inner shelf, although weaker than the stratification offshore, allows the cross-shelf circulation to extend over the inner shelf. As a result, upwelling is spread over a broader portion of the inner shelf than downwelling. In these along-shelf uniform model simulations, the inner shelf is less isolated from the middle shelf during upwelling- than during downwelling-favorable wind stresses.

There have been numerous observational studies characterizing the upwelling response over continental shelves (e.g., Smith 1981, Huyer 1990). More recently, a number of observational studies have examined the cross-shelf circulation over the inner shelf (Winant 1980, Churchill 1985, Lentz 1994, Munchow & Chant 2000, Garvine 2004, Liu & Weisberg 2005, Gutierrez et al. 2006, Estrade et al. 2008, Fewings et al. 2008). Two recent studies quantified the variation in the surface (and bottom) boundary-layer transport across the inner shelf (Lentz 2001, Kirincich et al. 2005). A compilation of estimates of normalized surface boundary-layer transport U^S/U^E as a function of water depth for both wide (east coast United States) and narrow (upwelling regions) continental shelves shows a consistent pattern for both stratified and unstratified conditions, although there are only a few estimates for unstratified flow (**Figure 4**). The dependence of U^S/U^E on water depth for the few estimates for unstratified flow is consistent with the Ekman model and a turbulent eddy-viscosity formulation. For stratified flow, the pattern is qualitatively similar to the Ekman (1905) response (**Figure 4**). In water depths greater than approximately 50 m, U^S approximately equals U^E . Onshore of the 50-m isobath, U^S/U^E decreases; it is near zero in 10-m water depth. The qualitative agreement between the average observed response and the classic Ekman model as well as the consistent dependence on water depth support the basic Ekman theory that the transport depends mainly on the ratio of the surface boundary-layer thickness to the water depth. Neither the offshore distance nor the baroclinic deformation radius collapses the observations. However, it is not clear in the observations what controls the cross-shelf structure of the average response in the stratified case. The average response shown in **Figure 4** does not shed light on whether there is an asymmetry in the stratified inner-shelf response to upwelling versus downwelling wind forcing, as suggested by along-shelf uniform numerical modeling studies and a few observations (**Figure 5**) (Weisberg et al. 2001, Austin & Lentz 2002, Liu & Weisberg 2007).

5.3. Cross-Shelf Wind Forcing

In contrast to along-shelf winds, cross-shelf winds are ineffective at driving along-shelf flows. Consequently, cross-shelf winds have been largely ignored in studies of wind-driven shelf circulation. However, as noted in Section 4 (see **Figure 2c**), in water depths of approximately 30 m or less, the cross-shelf wind stress is a substantial term in the cross-shelf momentum balance. Ekman's (1905) analysis shows that the cross-shelf wind can drive a cross-shelf circulation that extends all the way to the coast. The cross-shelf circulation due to cross-shelf winds is larger than the cross-shelf circulation due to along-shelf winds of the same magnitude in water depths that are less than the surface boundary-layer thickness δ_s . Models indicate that an onshore wind stress over an along-shelf uniform unstratified continental shelf forces a steady cross-shelf circulation that is confined to the surface boundary layer, with an onshore flow near the surface and an offshore return flow in the lower portion of the surface boundary layer (**Figure 6**) (Ekman 1905, Tilburg 2003).

In water deeper than the surface boundary-layer thickness, the circulation due to the cross-shelf wind stress is the one-dimensional (1D) open ocean Ekman response (Ekman 1905, Tilburg 2003).

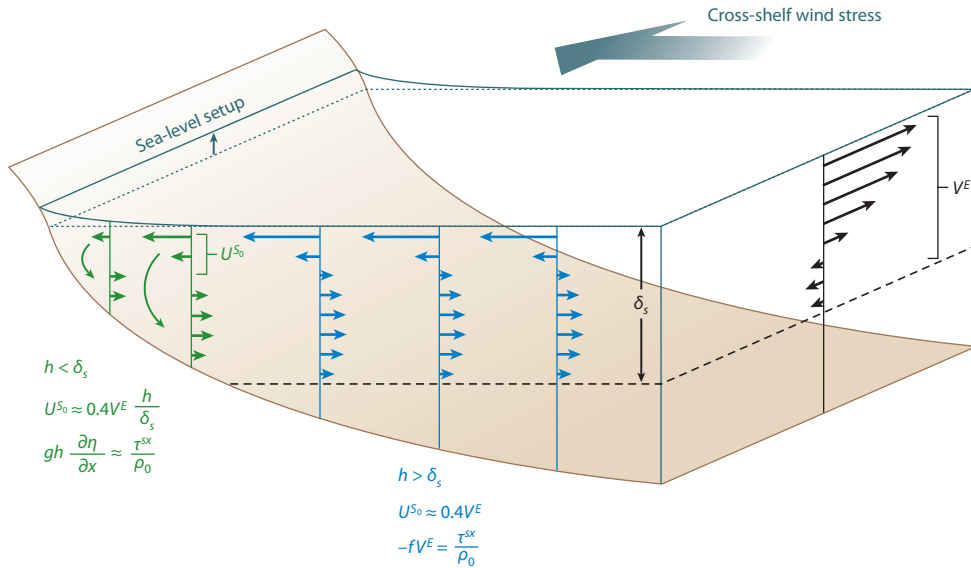


Figure 6

Schematic of the unstratified inner- and middle-shelf responses to a cross-shelf wind stress, highlighting two dynamical regions onshore and offshore of the location where the surface boundary layer intersects the bottom. The setup of the sea level is confined to the onshore region. The water depth is b , the surface boundary-layer thickness is δ_s , g is the acceleration due to gravity, η is the sea level, x is the cross-shelf coordinate, τ^{sx} is the cross-shelf wind stress, ρ_0 is the seawater density, f is the Coriolis parameter, the cross-shelf volume transport above the first zero crossing of the cross-shelf velocity profile is U^{S_0} , and the Ekman transport driven by the cross-shelf wind in deep water is $V^E = -\tau^{sx}/\rho_0 f$.

The circulation is confined to the surface boundary layer with a net along-shelf (perpendicular to the wind stress) Ekman transport $V^E = -\tau^{sx}/(\rho_0 f)$ and no net cross-shelf (downwind) transport in the surface boundary layer. As noted above, there is no cross-shelf pressure gradient in water deeper than the surface boundary layer because the cross-shelf wind forcing is entirely balanced by the Coriolis force within the surface boundary layer (Equation 18). There is a vertically sheared downwind flow in approximately the upper quarter of the surface boundary layer and a compensating upwind flow in the lower three-quarters of the surface boundary layer, depending on the form of the eddy viscosity used. The downwind transport in the upper part of the boundary layer (above the first zero crossing of the cross-shelf velocity profile) is $U^{S_0} \approx 0.4V^E$ ($0.32V^E$ for a constant eddy viscosity) (Tilburg 2003). In water deeper than δ_s , for a turbulent flow in which the eddy viscosity scales with u_* and z , the scaled velocities (u/u_*) are only a function of z/δ_{Et} .

Onshore of the region where the surface boundary layer intersects the bottom ($b < \delta_s$), the bottom stress reduces the along-shelf transport, and a cross-shelf pressure gradient develops to partially balance the cross-shelf wind stress. To a reasonable approximation, the Coriolis term associated with the along-shelf flow caused by cross-shelf wind forcing can be neglected in this region, and the cross-shelf momentum balance reduces to $\partial P/\partial x \approx \partial \tau^x/\partial z$ (see Section 4). [Note that if the along-shelf wind stress and along-shelf pressure gradient are not zero, as we assumed here, there may still be a substantial along-shelf flow and associated Coriolis term in this region (Figure 2c)]. In that case, the normalized velocity u/u_* is only a function of z/b . The cross-shelf current profile retains a similar structure to the offshore profile, with downwind (onshore) flow in the upper third of the water column and a compensating offshore flow in the lower two-thirds of the water

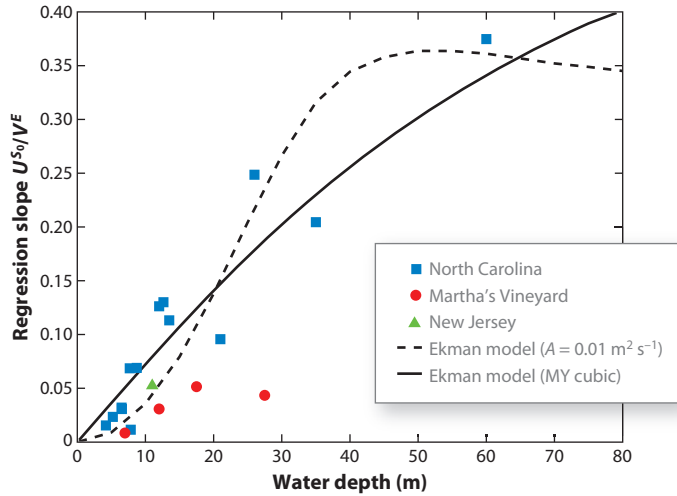


Figure 7

Linear regression slope between the observed cross-shelf transport (from the sea surface to the first zero crossing of the depth-varying part of the cross-shelf velocity) (U^{S_0}) and the Ekman transport estimated from the cross-shelf wind stress (V^E) as a function of water depth for three locations in the Middle Atlantic Bight. Estimates are also shown from an along-shelf uniform, unstratified model (Lentz 1995) for a constant eddy viscosity (A) and a cubic eddy viscosity (MY cubic) that resembles a Mellor-Yamada (Mellor & Yamada 1982) parameterization for unstratified flow (see Fewings et al. 2008).

column (**Figure 6**) (Tilburg 2003). Simple models indicate the corresponding downwind (and upwind) transport decreases linearly with decreasing water depth ($U^{S_0}/V^E \approx b/\delta_s$) (**Figure 7**).

The response of a stratified inner shelf to cross-shelf wind forcing has received even less attention than the case of an unstratified inner shelf. The response was examined by Tilburg (2003) using an along-shelf uniform numerical model. When the water column is stratified, the flow structure and the transports are similar to the unstratified case above because the downwind circulation is confined to the surface boundary layer, which is well mixed in density. The model indicates that the primary influence of stratification is to reduce the thickness of the surface boundary layer (in the offshore region where $\delta_s < b$) and hence the vertical shear in the circulation. The result is a factor-of-two reduction in the downwind transport U^{S_0} : from $0.3V^E$ for weak stratification ($N^2 = 10^{-5} \text{ s}^{-2}$), close to the unstratified value ($0.4V^E$), to $0.15V^E$ for strong stratification ($N^2 = 10^{-3} \text{ s}^{-2}$). In contrast to the case of along-shelf wind forcing, the model results exhibit no obvious asymmetry in the stratified response to onshore and offshore winds. This is not surprising, as the circulation is confined to the well-mixed surface layer, and consequently there are not substantial advective buoyancy fluxes.

Although a few observational studies have demonstrated the importance of the cross-shelf wind stress in the depth-averaged cross-shelf momentum balance (Lee et al. 1989, Lentz et al. 1999, Liu & Weisberg 2005, Fewings & Lentz 2010), there have been few studies examining the cross-shelf circulation driven by cross-shelf winds. One of the primary difficulties in observational studies is isolating the response to cross-shelf winds from the responses to along-shelf winds (see Section 5.2) and surface waves (see Section 5.4), as all three of these forcing terms are often correlated with each other. The response to cross-shelf winds can be isolated by taking advantage of a multiyear time series and considering only times when along-shelf wind stresses and surface gravity wave forcing are weak (Fewings et al. 2008). The observed cross-shelf velocity profiles during cross-shelf wind forcing are consistent with the profiles predicted by the along-shelf uniform Ekman model with a

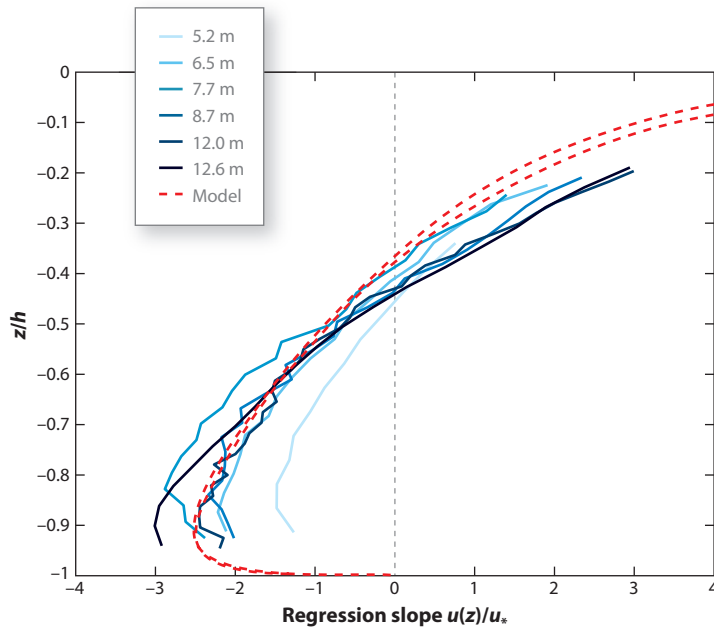


Figure 8

Profiles of the regression slope between the shear velocity $u_* = \sqrt{|\tau^{sx}|/\rho_0}$ based on the cross-shelf wind stress and cross-shelf currents u as a function of normalized depth (z/h) for six sites off North Carolina, spanning water depths from 5 m to 12.5 m. Also shown are the corresponding profiles from an along-shelf uniform, unstratified model (Lentz 1995) assuming a cubic eddy-viscosity profile for water depths of 5 and 13 m (red dashed curves). The cross-shelf wind stress is τ^{sx} , and ρ_0 is the seawater density.

constant or turbulent eddy viscosity (Cudaback et al. 2005, Fewings et al. 2008). Regression slopes between u_* based on cross-shelf wind stress and cross-shelf currents from six sites on the North Carolina shelf spanning water depths from 5 m to 12.5 m are consistent with along-shelf uniform model current profiles (**Figure 8**). Normalizing u by u_* and z by h also tends to collapse the profiles from different water depths, consistent with u/u_* being a function of z/h only, although there is more variation between the profiles than predicted by the model, particularly near the bottom.

A similar regression analysis between the along-shelf wind stress (or u_* based on τ^{sy}) and the cross-shelf current profiles from North Carolina indicates that there is no discernible response of the cross-shelf circulation to along-shelf winds in this water-depth range, consistent with previous modeling and observational results (Tilburg 2003, Fewings et al. 2008). There is also an observed increase in cross-shelf transport (above the first zero crossing in the cross-shelf velocity profile) with increasing cross-shelf wind stress consistent with the Ekman model dependence (Fewings et al. 2008). The results of Fewings et al. (2008) are extended in **Figure 7** by considering the regression slope between the observed cross-shelf transport U^{S_0} and the Ekman transport due to the cross-shelf wind stress V^E for sites in the Middle Atlantic Bight spanning water depths from 5 to 60 m. There is a linear increase in the regression slopes with increasing water depth toward a value of approximately $0.4V^E$ in deeper water, consistent with the model predictions (Ekman 1905, Tilburg 2003). The limited observational studies indicate that for unstratified inner shelves for which the cross-shelf wind stress is similar in magnitude to the along-shelf wind stress, cross-shelf wind forces a much larger cross-shelf circulation than does along-shelf wind in water depths that are less than the surface boundary-layer thickness (nominally ~ 20 m, by comparing

Figures 4 and 7). However, in contrast with Tilburg's (2003) model—in which stratification decreased the cross-shelf transport driven by cross-shelf winds—at an east coast site in 12-m water depth, the observed surface layer transport U^{S_0} is larger during the summer (stronger stratification) than during the winter (weak stratification) (Fewings et al. 2008). An important unresolved question is the impact stratification has on the inner-shelf response to cross-shelf winds.

5.4. Wave-Driven Circulation

The potential importance of surface gravity waves to the vertical structure of inner-shelf circulation has been considered only recently in models and observations (Xu & Bowen 1994, Fewings et al. 2008, Lentz et al. 2008, Kirincich et al. 2009, Uchiyama et al. 2010). The relationship between the depth-averaged cross-shelf flow and the Stokes drift, $\bar{u} \approx -\bar{u}_{st}$ (see Section 2.2), depends only on the assumptions of an onshore Stokes transport due to the waves and the assumption that there are no along-shelf variations in the flow. That relationship does not indicate whether the offshore flow is dynamically associated with radiation stresses or Stokes-Coriolis forcing.

Xu & Bowen (1994) first considered the implications of the Stokes-Coriolis force for wave-driven flows over the inner shelf in a 1D model of shallow-water flow. Building on their model, Lentz et al. (2008) examined wave-driven flow in a simple along-shelf uniform model that included a coastal boundary, onshore Stokes drift transport due to the waves, the cross-shelf setup of the sea level, and wave-radiation stresses. That model suggests that the structure of the wave-driven cross-shelf circulation depends on the strength of the vertical mixing. For strong vertical mixing, the cross-shelf current profiles are parabolic with the maximum offshore flow at mid-depth, similar to what is observed in the surf zone (Haines & Sallenger 1994, Garcez Faria et al. 2000, Reniers et al. 2004). For weak vertical mixing, the offshore flow is equal in magnitude but opposite in direction to the Stokes drift velocity [$u(z) = -u_{st}(z)$], with the strongest offshore flow near the surface (**Figure 9**).

Over the Massachusetts, North Carolina, and Oregon inner shelves, the observed offshore velocity profiles in the absence of wind forcing do have the same vertical structure as, but are opposite in direction to, the Stokes drift-velocity profile (Equation 3): $u(z) = -u_{st}(z)$, consistent with Stokes-Coriolis forcing of the cross-shelf flow and weak vertical mixing over the inner shelf relative to the surf zone (Lentz et al. 2008, Kirincich et al. 2009). The tendency for the offshore flow forced by the waves to be equal in magnitude to the onshore Stokes drift velocity at each depth suggests that surface wave forcing results in nearly zero net cross-shelf Lagrangian transport of passive particles over the inner shelf. The agreement between the observed profiles and the model response with no vertical mixing suggests that stratification should have no impact on the wave-driven flow, as the vertical mixing cannot be reduced further. However, preliminary observations suggest an enhanced vertical shear in the wave-driven offshore flow when the water column is stratified (Lentz et al. 2008). How stratification would influence the wave-driven flow remains a mystery.

5.5. Combined Wind and Wave Forcing

Above we examine wind and wave forcing in isolation to describe how each contributes to the inner-shelf circulation and coastal setup. However, wind and wave forcing typically occur simultaneously and are correlated with each other. This is particularly true for cross-shelf winds and waves. Onshore winds (blowing toward land) are usually associated with relatively large surface waves due to the large fetch allowing the waves to grow. The wave-driven undertow $u(z) \approx -u_{st}(z)$ is offshore and vertically sheared, with the maximum flow near the surface. The wind-driven circulation is

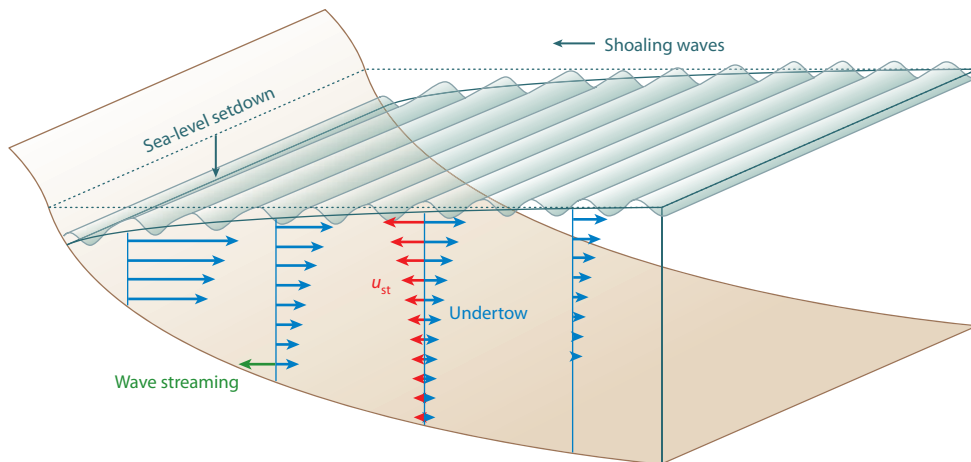


Figure 9

Schematic of the inner-shelf circulation forced by surface gravity waves, showing the response to Stokes-Coriolis forcing (*blue*) and wave-induced bottom streaming (*green*). Note that the surf zone and middle shelf are not shown. The Stokes drift (*red*) is not detected by Eulerian (fixed in space) measurements, such as those from acoustic Doppler current profilers, but is added to Eulerian measurements to estimate the net Lagrangian transport. Over the inner shelf, the Stokes drift $u_{st}(z)$ tends to cancel the Stokes-Coriolis-induced Eulerian velocity or undertow, suggesting that the net wave-driven transport is near zero over most of the water column.

also vertically sheared but is onshore near the surface and offshore near the bottom. The vertical shears of the wave- and wind-driven flows tend to cancel; the combination of onshore winds and large waves results in observed (Eulerian) cross-shelf flows with little shear (Fewings et al. 2008). Offshore winds (blowing from land toward the ocean) are typically associated with smaller surface waves because of the limited fetch. If there are offshore winds and onshore propagating waves, the vertical shears add and result in an observed cross-shelf flow that is strongly vertically sheared, with offshore flow near the surface and onshore flow near the bottom. The tendency for onshore winds to be associated with larger waves than offshore winds leads to an apparent asymmetry in the wind-driven circulation if the effect of waves is not taken into account.

6. FUTURE DIRECTIONS

Recent advances in theoretical understanding, instrumentation, and numerical modeling provide a basis for rapid progress in the near future in understanding inner-shelf circulation and dynamics.

6.1. Direct Measurement of Stresses

Turbulent stresses are a central element of inner-shelf dynamics that control the structure and strength of wind- and wave-driven flow, but direct covariance measurements of turbulent stresses are difficult to make in the presence of typical inner-shelf surface gravity wave forcing. Covariance stress estimates have now been made in the bottom boundary layer (Shaw & Trowbridge 2001), in the surface boundary layer (Gerbi et al. 2008), and throughout most of the water column using acoustic Doppler current profilers (Rosman et al. 2008, Kirincich et al. 2010). Future measurements of turbulent stress profiles should substantially improve our understanding of inner-shelf

dynamics, particularly in stratified regions. A better understanding of bottom stress dynamics over the inner shelf is needed (see Section 3.1) not only for improving models of the circulation, but also for understanding processes such as sediment transport across the inner shelf. Direct measurements of near-bottom turbulent stresses at inner-shelf sites will help determine the local bottom stress, evaluate existing wave-current interaction models of bottom stress, and refine our understanding of how the bottom stress depends on surface waves, evolving bedforms, and near-bed stratification.

6.2. Numerical Simulations of Wave Forcing

Numerical models that incorporate surface gravity wave forcing are now being constructed and tested (e.g., McWilliams et al. 2004, Newberger & Allen 2006, Ardhuin et al. 2008, Mellor 2008, Warner et al. 2008, Uchiyama et al. 2010). There are terms in the momentum balances involving interactions between the wave and mean flows that may be substantial over the inner shelf but are not included in Equations 6 and 14 for simplicity and because those terms have not been addressed in observational studies. Numerical modeling process studies will provide insight into the effects of those wave forcing terms and guide future observational studies to evaluate the numerical model results. The appropriate surface and bottom boundary conditions in the presence of waves are also the subject of active research.

6.3. Three-Dimensional Circulation

The relative importance of 3D cross-shelf exchange in comparison with 2D exchange is not established. Most studies of cross-shelf transport and exchange over the inner shelf have focused on 2D exchange: coastal upwelling and downwelling. In 3D flows, the depth-averaged cross-shelf velocity is not constrained to be zero because the circulation is not along-shelf uniform (Tilburg & Garvine 2003, Kirincich & Barth 2009). The cross-shelf flow is large in regions where divergence in the along-shelf flow is large (see Section 2.1). Complex coastline topography—any coastline that is not straight, as in the along-shelf uniform models discussed in this review—will lead to divergence in the along-shelf and cross-shelf flows and may drive substantial horizontal cross-shelf exchange. A key advance is the growing network of high-frequency coastal radar systems that can now provide maps of the surface flow field with horizontal resolutions of tens of kilometers to hundreds of meters, depending on the particular unit (e.g., Paduan & Rosenfeld 1996, Emery et al. 2004, Kosro 2005, Dzwonkowski et al. 2009, Kim 2010). Resolving the spatial variability of the subsurface flow remains a challenge and still may require closely spaced 3D arrays of instruments. Numerical models are now becoming available that reveal complex circulation on spatial scales of tens of meters to kilometers (e.g., Newberger & Allen 2006, Warner et al. 2008, Uchiyama et al. 2010). The cross-shelf depth-averaged flow in such a complex circulation may drive cross-shelf transport as substantial as that due to coastal upwelling and downwelling.

Traditionally, cross-shelf winds and surface gravity waves have not been considered in continental-shelf circulation studies. The recent observational and modeling studies reviewed in this article highlight the importance of cross-shelf winds and surface gravity waves in forcing inner-shelf circulation.

DISCLOSURE STATEMENT

The authors are not aware of any affiliations, memberships, funding, or financial holdings that might be perceived as affecting the objectivity of this review.

ACKNOWLEDGMENTS

The authors thank J. Trowbridge and C. Tilburg for helpful discussions. A. Kirincich provided the Oregon data, which were collected by the Partnership for Interdisciplinary Studies of Coastal Oceans, a long-term ecological consortium funded primarily by the Gordon and Betty Moore Foundation and David and Lucile Packard Foundation. Peter Howd and Kent Hathaway provided the North Carolina data, which were collected as part of the SandyDuck '97 experiment funded by the U.S. Army Corps of Engineers, the Office of Naval Research, and the U.S. Geological Survey. This study was supported by NSF grants OCE-0548961, OCE-0751554, and OCE-0957948.

LITERATURE CITED

- Allen SE, Durrieu de Madron X. 2009. A review of the role of submarine canyons in deep-ocean exchange with the shelf. *Ocean Sci.* 5:607–20
- Allen JS, Newberger PA. 1996. Downwelling circulation on the Oregon continental shelf. Part I: response to idealized forcing. *J. Phys. Oceanogr.* 26:2011–35
- Allen JS, Newberger PA, Federiuk J. 1995. Upwelling circulation on the Oregon continental shelf. Part I: response to idealized forcing. *J. Phys. Oceanogr.* 25:1843–66
- Ardhuin F, Chapron B, Elfouhaily T. 2004. Waves and the air-sea momentum budget: implications for ocean circulation modeling. *J. Phys. Oceanogr.* 34:1741–55
- Ardhuin F, Herbers THC, O'Reilly WC. 2001. A hybrid Eulerian-Lagrangian model for spectral wave evolution with application to bottom friction on the continental shelf. *J. Phys. Oceanogr.* 31:1498–516
- Ardhuin F, Rasche N, Belibassakis KA. 2008. Explicit wave-averaged primitive equations using a generalized Lagrangian mean. *Ocean Model.* 32:35–60
- Atkinson LP, Brink KH, Davis RE, Jones BH, Paluszkiwicz T, Stuart DW. 1986. Mesoscale hydrographic variability in the vicinity of Points Conception and Arguello during April-May 1983: the OPUS 1983 experiment. *J. Geophys. Res.* 91:12899–918
- Austin JA, Barth JA. 2002. Drifter behavior on the Oregon-Washington shelf during downwelling-favorable winds. *J. Phys. Oceanogr.* 32:3132–44
- Austin JA, Lentz SJ. 2002. The inner shelf response to wind-driven upwelling and downwelling. *J. Phys. Oceanogr.* 32:2171–93
- Bowen AJ, Inman DL, Simmons VP. 1968. Wave 'set-down' and set-up. *J. Geophys. Res.* 73:2569–77
- Brown WS, Irish JD, Winant CD. 1987. A description of subtidal pressure field observations on the northern California shelf during the Coastal Ocean Dynamics Experiment. *J. Geophys. Res.* 92:1605–36
- Brown WS, Pettigrew NR, Irish JD. 1985. The Nantucket Shoals Flux Experiment (NSFE79). Part II: the structure and variability of across-shelf pressure gradients. *J. Phys. Oceanogr.* 15:749–71
- Churchill JH. 1985. Properties of flow within the coastal boundary layer off Long Island, New York. *J. Phys. Oceanogr.* 15:898–916
- Choboter PF, Duke D, Horton JP, Sinz P. 2011. Exact solutions of wind-driven coastal upwelling and downwelling over sloping topography. *J. Phys. Oceanogr.* 41:1277–96
- Choboter PF, Samelson RM, Allen JS. 2005. A new solution of a nonlinear model of upwelling. *J. Phys. Oceanogr.* 35:532–44
- Cudaback CN, Washburn L, Dever E. 2005. Subtidal inner-shelf circulation near Point Conception. *J. Geophys. Res.* 110:C10007
- Davies AG, Villaret C. 1999. Eulerian drift induced by progressive waves above rippled and very rough beds. *J. Geophys. Res.* 104:1465–88
- Dever EP. 1997. Wind-forced cross-shelf circulation on the northern California shelf. *J. Phys. Oceanogr.* 27:1566–80
- Drinkwater KF. 1989. The response of an open embayment to near-hurricane force winds. *Cont. Shelf. Res.* 9:823–39
- Dudas SE, Grantham BA, Kirincich AR, Menge BA, Lubchenco J, Barth JA. 2009. Current reversals as determinants of intertidal recruitment on the central Oregon coast. *ICES J. Mar. Sci.* 66:396–407

- Dzwonkowski B, Kohut JT, Yan X-H. 2009. Seasonal differences in wind-driven across-shelf forcing and response relationships in the shelf surface layer of the central Mid-Atlantic Bight. *J. Geophys. Res.* 114:C08018
- Ekman VW. 1905. On the influence of the Earth's rotation on ocean-currents. *Ark. Mat. Aston. Fys.* 2:1-53
- Emery BM, Washburn L, Harlan JA. 2004. Evaluating radial current measurements from CODAR high-frequency radars with moored current meters. *J. Atmos. Ocean. Technol.* 21:1259-71
- Epifanio CE, Garvine RW. 2001. Larval transport on the Atlantic continental shelf of North America: a review. *Estuar. Coast. Shelf Sci.* 52:51-77
- Estrade P, Marchesiello P, de Verdiere AC, Roy C. 2008. Cross-shelf structure of coastal upwelling: a two-dimensional extension of Ekman's theory and a mechanism for inner shelf upwelling shut down. *J. Mar. Res.* 66:589-616
- Falkowski PG, Barber RT, Smetacek V. 1998. Biogeochemical controls and feedbacks on ocean primary production. *Science* 281:200-6
- Fewings MR, Lentz SJ. 2010. Momentum balances on the inner continental shelf at Martha's Vineyard Coastal Observatory. *J. Geophys. Res.* 115:C12023
- Fewings MR, Lentz SJ, Fredericks J. 2008. Observations of cross-shelf flow driven by cross-shelf winds on the inner continental shelf. *J. Phys. Oceanogr.* 38:2358-78
- Garcez Faria AF, Thornton EB, Lippman TC, Stanton TP. 2000. Undertow over a barred beach. *J. Geophys. Res.* 105:16999-7010
- Garland ED, Zimmer CA, Lentz SJ. 2002. Larval distributions in inner-shelf waters: the roles of wind-driven cross-shelf currents and diel vertical migrations. *Limnol. Oceanogr.* 47:803-17
- Garvine RW. 2004. The vertical structure and subtidal dynamics of the inner shelf off New Jersey. *J. Mar. Res.* 62:337-71
- Gerbi GP, Trowbridge JH, Edson JB, Plueddemann AJ, Terray EA, Fredericks JJ. 2008. Measurements of momentum and heat transfer across the air-sea interface. *J. Phys. Oceanogr.* 38:1054-72
- Glenn SM, Grant WD. 1987. A suspended sediment stratification correction for combined wave and current flows. *J. Geophys. Res.* 92:8244-46
- Grant WD, Madsen OS. 1979. Combined wave and current interaction with a rough bottom. *J. Geophys. Res.* 84:1797-808
- Grant WD, Madsen OS. 1982. Movable bed roughness in unsteady oscillatory flow. *J. Geophys. Res.* 87:469-81
- Grant WD, Madsen OS. 1986. The continental-shelf bottom boundary layer. *Annu. Rev. Fluid Mech.* 18:265-305
- Grantham BA, Chan F, Nielsen KJ, Fox DS, Barth JA, et al. 2004. Upwelling-driven nearshore hypoxia signals ecosystem and oceanographic changes in the northeast Pacific. *Nature* 429:749-54
- Gutierrez BT, Voulgaris G, Work PA. 2006. Cross-shore variations of wind-driven flows on the inner shelf in Long Bay, South Carolina, United States. *J. Geophys. Res.* 111:C03015
- Haines JW, Sallenger AH Jr. 1994. Vertical structure of mean cross-shore currents across a barred surf zone. *J. Geophys. Res.* 99:14223-42
- Hasselmann K. 1970. Wave-driven inertial oscillations. *Geophys. Fluid Dyn.* 1:463-502
- Herbers THC, Hendrickson EJ, O'Reilly WC. 2000. Propagation of swell across a wide continental shelf. *J. Geophys. Res.* 108:19729-37
- Hickey BM, Dobbins EL, Allen SE. 2003. Local and remote forcing of currents and temperature in the central Southern California Bight. *J. Geophys. Res.* 108:C3081
- Huyer A. 1990. Shelf circulation. In *The Sea*, Vol. 9A, ed. B LeMehaute, DM Hanes, pp. 345-93. New York: Wiley
- Keen TR, Glenn SM. 1994. A coupled hydrodynamic-bottom boundary layer model of Ekman flow on stratified continental shelves. *J. Phys. Oceanogr.* 24:1732-49
- Kim SY. 2010. Observations of submesoscale eddies using high-frequency radar-derived kinematic and dynamic quantities. *Cont. Shelf Res.* 30:1639-55
- Kirincich AR, Barth JA. 2009. Along-shelf variability of inner-shelf circulation along the Central Oregon coast during summer. *J. Phys. Oceanogr.* 39:1380-98
- Kirincich AR, Barth JA, Grantham BA, Menge BA, Lubchenco J. 2005. Wind-driven inner-shelf circulation off Oregon during summer. *J. Geophys. Res.* 110:C10S03

- Kirincich AR, Lentz SJ, Barth JA. 2009. Wave-driven inner-shelf motions on the Oregon coast. *J. Phys. Oceanogr.* 39:2942–56
- Kirincich AR, Lentz SJ, Gerbi GP. 2010. Calculating Reynolds stresses from ADCP measurements in the presence of surface gravity waves using the cospectra-fit method. *J. Atmos. Ocean. Technol.* 27:889–907
- Kosro PM. 2005. On the spatial structure of coastal circulation off Newport, Oregon, during spring and summer 2001 in a region of varying shelf width. *J. Geophys. Res.* 110:C10S06
- Kundu PK, Allen JS. 1976. Some three-dimensional characteristics of low-frequency current fluctuations near the Oregon coast. *J. Phys. Oceanogr.* 6:181–99
- Lane EM, Restrepo JM, McWilliams JC. 2007. Wave-current interaction: a comparison of radiation-stress and vortex-force representations. *J. Phys. Oceanogr.* 37:1122–41
- Lee TN, Ho WJ, Kourafalou V, Wang JD. 1984. Circulation on the continental shelf of the southeastern United States. Part I: subtidal response to wind and Gulf Stream forcing during winter. *J. Phys. Oceanogr.* 14:1001–12
- Lee TN, Williams E, Wang REJ, Atkinson L. 1989. Response of South Carolina continental shelf waters to wind and Gulf Stream forcing during winter of 1986. *J. Geophys. Res.* 94:10715–54
- Lentz SJ. 1992. The surface boundary layer in coastal upwelling regions. *J. Phys. Oceanogr.* 22:1517–39
- Lentz SJ. 1994. Current dynamics over the northern California inner shelf. *J. Phys. Oceanogr.* 24:2461–78
- Lentz SJ. 1995. Sensitivity of the inner-shelf circulation to the eddy-viscosity profile. *J. Phys. Oceanogr.* 25:19–28
- Lentz SJ. 2001. The influence of stratification on the wind-driven cross-shelf circulation over the North Carolina shelf. *J. Phys. Oceanogr.* 31:2749–60
- Lentz SJ, Fewings M, Howd P, Fredericks J, Hathaway K. 2008. Observations and a model of undertow over the inner continental shelf. *J. Phys. Oceanogr.* 38:2341–57
- Lentz SJ, Guza RT, Elgar S, Feddersen F, Herbers THC. 1999. Momentum balances on the North Carolina inner shelf. *J. Geophys. Res.* 104:18205–26
- Lentz SJ, Winant CD. 1986. Subinertial currents on the southern California shelf. *J. Phys. Oceanogr.* 16:1737–50
- Liu Y, Weisberg RH. 2005. Momentum balance diagnoses for the West Florida Shelf. *Cont. Shelf Res.* 25:2054–74
- Liu Y, Weisberg RH. 2007. Ocean currents and sea surface heights estimated across the West Florida Shelf. *J. Phys. Oceanogr.* 37:1697–713
- Longuet-Higgins MS. 1953. On wave set-up in shoaling water with a rough sea bed. *J. Fluid Mech.* 527:217–34
- Longuet-Higgins MS. 2005. Mass transport in water waves. *Philos. Trans. R. Soc. Lond. Ser. A* 245:535–81
- Longuet-Higgins MS, Stewart RW. 1962. Radiation stresses in water waves: a physical discussion, with applications. *Deep Sea Res.* 11:529–62
- Longuet-Higgins MS, Stewart RW. 1964. Radiation stresses and mass transport in gravity waves, with application to “surf-beats.” *J. Fluid Mech.* 13:481–504
- Madsen OS. 1977. A realistic model of the wind-induced Ekman boundary layer. *J. Phys. Oceanogr.* 7:248–55
- McWilliams JC, Restrepo JM. 1999. The wave-driven ocean circulation. *J. Phys. Oceanogr.* 29:2523–40
- McWilliams JC, Restrepo JM, Lane EM. 2004. An asymptotic theory for the interaction of waves and currents in coastal waters. *J. Fluid Mech.* 511:135–78
- Mei CC. 1983. *The Applied Dynamics of Ocean Surface Waves*. New York: McGraw-Hill
- Mellor G. 2003. The three-dimensional current and surface wave equations. *J. Phys. Oceanogr.* 33:1978–89
- Mellor GL. 2008. The depth-dependent current and wave interaction equations: a revision. *J. Phys. Oceanogr.* 38:2587–96
- Mellor GL, Yamada T. 1982. Development of a turbulence closure model for geophysical fluid problems. *Rev. Geophys. Space Phys.* 20:851–75
- Munchow A, Chant RJ. 2000. Kinematics of inner shelf motions during the summer stratified season off New Jersey. *J. Phys. Oceanogr.* 30:247–68
- Newberger PA, Allen JS. 2006. Forcing a three-dimensional, hydrostatic primitive-equation model for application in the surf zone, part 1: formulation. *J. Geophys. Res.* 112:C08018
- Nittrouer CA, Wright LD. 1994. Transport of particles across continental shelves. *Rev. Geophys.* 32:85–113

- Noble M, Butman B, Williams E. 1983. On the longshore structure and dynamics of subtidal currents on the eastern United States continental shelf. *J. Phys. Oceanogr.* 13:2125–47
- Nof D, Paldor N. 1992. Are there oceanographic explanations for the Israelites crossing the Red Sea? *Bull. Am. Meteorol. Soc.* 73:305–14
- Paduan, JD, Rosenfeld LK. 1996. Remotely sensed surface currents in Monterey Bay from shore-based HF radar (Coastal Ocean Dynamics Application Radar). *J. Geophys. Res.* 101:20669–86
- Pedlosky J. 1978. An inertial model of steady coastal upwelling. *J. Phys. Oceanogr.* 8:171–77
- Phillips OM. 1980. *The Dynamics of the Upper Ocean*. Cambridge, UK: Cambridge Univ. Press
- Poon YK, Madsen OS. 1991. A two-layer wind-driven coastal circulation model. *J. Geophys. Res.* 96:2535–48
- Raubenheimer R, Guza RT, Elgar S. 2001. Field observations of wave-driven setdown and setup. *J. Geophys. Res.* 106:4629–38
- Reniers AJHM, Thornton EB, Stanton TP, Roelvink JA. 2004. Vertical flow structure during Sandy Duck: observations and modeling. *Coastal Eng.* 51:237–60
- Rosman J, Hench J, Koseff J, Monismith S. 2008. Extracting Reynolds stresses from acoustic Doppler current profiler measurements in wave-dominated environments. *J. Atmos. Ocean. Technol.* 25:286–306
- Scott JT, Csanady GT. 1976. Nearshore currents off Long Island. *J. Geophys. Res.* 81:5401–9
- Shaw WJ, Trowbridge JH. 2001. The direct estimation of near-bottom turbulent fluxes in the presence of energetic wave motions. *J. Atmos. Ocean. Technol.* 18:1540–57
- Shearman RK, Lentz SJ. 2003. Dynamics of mean and subtidal flow on the New England shelf. *J. Geophys. Res.* 108:3281
- Smith RL. 1981. A comparison of the structure and variability of the flow field in three coastal upwelling regions: Oregon, Northwest Africa, and Peru. In *Coastal Upwelling*, ed. FA Richards, pp. 107–18. Washington, DC: Am. Geophys. Union
- Smith JA. 2006. Wave-current interactions in finite depth. *J. Phys. Oceanogr.* 36:1403–19
- Stokes GG. 1847. On the theory of oscillatory waves. *Trans. Camb. Philos. Soc.* 8:441–55
- Styles R, Glenn SM. 2000. Modeling stratified wave and current bottom boundary layers on the continental shelf. *J. Geophys. Res.* 105:24119–39
- Thomas JH. 1975. A theory of steady wind-driven currents in shallow water with variable eddy viscosity. *J. Phys. Oceanogr.* 5:136–42
- Thornton EB, Guza RT. 1986. Surf zone longshore currents and random waves: field data and models. *J. Phys. Oceanogr.* 16:1165–78
- Tilburg CE. 2003. Across-shelf transport on a continental shelf: Do across-shelf winds matter? *J. Phys. Oceanogr.* 33:2675–88
- Tilburg CE, Garvine RW. 2003. Three-dimensional flow in a shallow coastal upwelling zone: alongshore convergence and divergence on the New Jersey shelf. *J. Phys. Oceanogr.* 33:2113–25
- Tilburg CE, Garvine RW. 2004. A simple model for coastal sea level prediction. *Weather Forecast.* 19:511–19
- Traykovski P. 2007. Observations of wave orbital scale ripples and a nonequilibrium time-dependent model. *J. Geophys. Res.* 112:C06026
- Uchiyama Y, McWilliams JC, Shchepetkin AF. 2010. Wave-current interaction in an oceanic circulation model with a vortex-force formalism: application to the surf zone. *Ocean Model.* 34:16–35
- Ursell F. 1950. On the theoretical form of ocean swell on a rotating earth. *Mon. Not. R. Astron. Soc. Geophys. Suppl.* 6:1–8
- Warner JC, Sherwood CR, Signell RP, Harris CK, Arango HG. 2008. Development of a three-dimensional, regional, coupled wave, current, and sediment transport model. *Comput. Geosci.* 34:1284–306
- Weisberg RH, Li Z, Muller-Karger F. 2001. West Florida shelf response to local wind forcing: April 1998. *J. Geophys. Res.* 106:31239–62
- Wiberg PL, Harris K. 1994. Ripple geometry in wave-dominated environments. *J. Geophys. Res.* 99:775–89
- Wiberg PL, Smith JD. 1983. A comparison of field data and theoretical models for wave-current interactions at the bed on the continental shelf. *Cont. Shelf Res.* 2:147–62
- Winant CD. 1980. Downwelling over the Southern California shelf. *J. Phys. Oceanogr.* 10:791–99

- Winant CD, Beardsley RC, Davis RE. 1987. Moored wind, temperature, and current observations made during Coastal Ocean Dynamics Experiments 1 and 2 over the northern California continental shelf and upper slope. *J. Geophys. Res.* 92:1569–604
- Woodson CB, Washburn L, Barth JA, Hoover DJ, Kirincich AR, et al. 2009. Northern Monterey Bay upwelling shadow front: observations of a coastally and surface-trapped buoyant plume. *J. Geophys. Res.* 114:C12013
- Xu Z, Bowen AJ. 1994. Wave- and wind-driven flow in water of finite depth. *J. Phys. Oceanogr.* 24:1850–66
- Yankovsky AE, Garvine RW. 1998. Subinertial dynamics on the inner New Jersey shelf during the upwelling season. *J. Phys. Oceanogr.* 28:2444–58
- Zou Q, Bowen AJ, Hay AE. 2006. Vertical distribution of wave shear stress in variable water depth: theory and field observations. *J. Geophys. Res.* 111:C09032



Contents

A Conversation with Karl K. Turekian <i>Karl K. Turekian and J. Kirk Cochran</i>	1
Climate Change Impacts on Marine Ecosystems <i>Scott C. Doney, Mary Ruckelshaus, J. Emmett Duffy, James P. Barry, Francis Chan, Chad A. English, Heather M. Galindo, Jacqueline M. Grebmeier, Anne B. Hollowed, Nancy Knowlton, Jeffrey Polovina, Nancy N. Rabalais, William J. Sydeman, and Lynne D. Talley</i>	11
The Physiology of Global Change: Linking Patterns to Mechanisms <i>George N. Somero</i>	39
Shifting Patterns of Life in the Pacific Arctic and Sub-Arctic Seas <i>Jacqueline M. Grebmeier</i>	63
Understanding Continental Margin Biodiversity: A New Imperative <i>Lisa A. Levin and Myriam Sibuet</i>	79
Nutrient Ratios as a Tracer and Driver of Ocean Biogeochemistry <i>Curtis Deutsch and Thomas Weber</i>	113
Progress in Understanding Harmful Algal Blooms: Paradigm Shifts and New Technologies for Research, Monitoring, and Management <i>Donald M. Anderson, Allan D. Cembella, and Gustaaf M. Hallegraeff</i>	143
Thin Phytoplankton Layers: Characteristics, Mechanisms, and Consequences <i>William M. Durham and Roman Stocker</i>	177
Jellyfish and Ctenophore Blooms Coincide with Human Proliferations and Environmental Perturbations <i>Jennifer E. Purcell</i>	209
Benthic Foraminiferal Biogeography: Controls on Global Distribution Patterns in Deep-Water Settings <i>Andrew J. Gooday and Frans J. Jorissen</i>	237

Plankton and Particle Size and Packaging: From Determining Optical Properties to Driving the Biological Pump <i>L. Stemann and E. Boss</i>	263
Overturning in the North Atlantic <i>M. Susan Lozier</i>	291
The Wind- and Wave-Driven Inner-Shelf Circulation <i>Steven J. Lentz and Melanie R. Fewings</i>	317
Serpentinite Mud Volcanism: Observations, Processes, and Implications <i>Patricia Fryer</i>	345
Marine Microgels <i>Pedro Verdugo</i>	375
The Fate of Terrestrial Organic Carbon in the Marine Environment <i>Neal E. Blair and Robert C. Aller</i>	401
Marine Viruses: Truth or Dare <i>Mya Breitbart</i>	425
The Rare Bacterial Biosphere <i>Carlos Pedrós-Alió</i>	449
Marine Protistan Diversity <i>David A. Caron, Peter D. Countway, Adriane C. Jones, Diane Y. Kim, and Astrid Schnetzer</i>	467
Marine Fungi: Their Ecology and Molecular Diversity <i>Thomas A. Richards, Meredith D.M. Jones, Guy Leonard, and David Bass</i>	495
Genomic Insights into Bacterial DMSP Transformations <i>Mary Ann Moran, Chris R. Reisch, Ronald P. Kiene, and William B. Whitman</i>	523

Errata

An online log of corrections to *Annual Review of Marine Science* articles may be found at <http://marine.annualreviews.org/errata.shtml>